Minimum Junction Temperature Swing for DFIG to Ride Through Symmetrical Voltage Dips

Zhou, Dao; Blaabjerg, Frede

Published in:
Proceedings of the 2015 IEEE Energy Conversion Congress and Exposition (ECCE)

DOI (link to publication from Publisher):
10.1109/ECCE.2015.7309729

Publication date:
2015

Minimum Junction Temperature Swing for DFIG to Ride Through Symmetrical Voltage Dips

Dao Zhou, Frede Blaabjerg
Department of Energy Technology
Aalborg University
Aalborg, Denmark
zda@et.aau.dk; fbl@et.aau.dk

***Abstract* — Doubly-Fed Induction Generator (DFIG) system is popular for wind turbines above 1 MW. Existing issues for a DFIG system to ride through a symmetrical grid fault are addressed in terms of the internal and external challenges. Based on the conventional demagnetizing current control, the design procedure of an optimum demagnetizing coefficient is proposed considering the reactive current injection required by the modern grid codes, which guarantees same maximum rotor current between the fault occurrence and the duration of the reactive current injection. As the thermal behavior of the power semiconductor is mainly decided by its current, the minimum junction temperature swing can be achieved by using this control strategy. It is concluded that, regardless of the rotor speed, the demagnetizing coefficient is only related to the dip level. Compared with the traditional vector control, simulation results agree with the reduced junction temperature swing during fault period.**

I. INTRODUCTION

A recent study by the Danish Energy Agency indicates that onshore wind power is the cheapest form of new electricity generation in Denmark [1]. Meanwhile, due to the noise emission, footprint limitation and richer wind energy, it is promising to move the wind turbines offshore, whose lifespan is prolonged to 20-25 years [2]. As one of the most vulnerable components of the wind turbine system, more and more efforts have been devoted to the reliable behavior of the power electronic converter because of the increased cost and time for offshore maintenance [3]. Furthermore, it is generally accepted that the thermal profile of the power semiconductor is an important indicator of the lifetime, and it has an influence on the reliability metrics [4], [5].

The Doubly-Fed Induction Generator (DFIG) is a widely used configuration for wind turbines above 1 MW. It provides the advantage of variable speed operation and full control active and reactive power using a converter with only a small fraction of the rated power (20%-30%) [6]. However, on detecting a grid fault, the generator unit is usually disconnected to protect the vulnerable rotor-side converter by using the crowbar [7]. This approach makes the DFIG as a traditional squirrel-cage motor, absorbing the reactive power from the grid which is against the modern grid codes [8], [9]. Another hardware solution for the fault ride-through operation is applying the dc-chopper to prevent the dc-link over-voltage [10]. On the other hand, many studies have been conducted to overcome the grid fault viewed from a software solution with the advantages of reduced cost and easy implementation [11]-[13]. Among them, demagnetizing control is a popular solution, whose target is switched from the maximum power tracking to the natural stator flux elimination. Due to the assumption that the natural stator flux should be removed as soon as possible, the demagnetizing coefficient is designed at the maximum rating of the rotor current [11]. However, it is not the best solution viewed from the transient thermal performance of the power semiconductor, which is also closely related to the reliability of the long-term operational wind turbine system. Considering the low voltage ride-through requirement from modern grid codes, this paper will propose an optimized design of the demagnetizing coefficient, which is aimed at minimum junction temperature swing during the fault period.

The structure of this paper is organized as follows. Section II addresses the internal and external challenges to overcome the grid fault. Then, the capability of the DFIG facing the symmetrical voltage dip is analyzed and calculated in section III. Besides, the control strategy for the minimum thermal stress of the power converter is evaluated and studied in section IV. Simulation validations are performed in section V, and some concluding remarks are drawn in the last section.

II. EXISTING ISSUES FACING SYMMETRICAL GRID FAULTS

A typical DFIG system is depicted in Fig. 1, in which a dc-brake is alternatively employed to realize the low voltage ride-through. As the stator of the induction generator is directly linked to the grid, the stator flux cannot be changed abruptly, when the grid fault occurs. Correspondingly, the component of the stator flux can be divided into the positive stator flux and natural stator flux in the case of the symmetrical voltage sag, while an extra negative component is introduced during the asymmetrical grid fault [12]. For simplicity, this paper only analyzes and deals with the symmetrical grid voltage dip.

978-1-4673-7151-3/15/$31.00 ©2015 IEEE

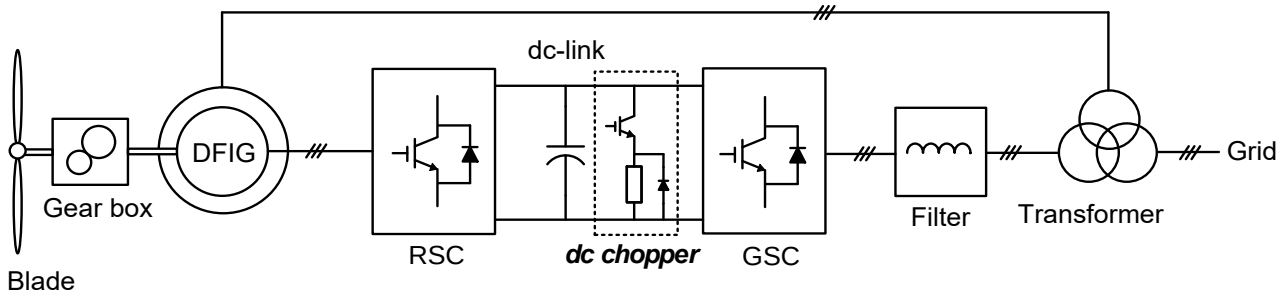

Fig. 1. Doubly-Fed Induction Generator (DFIG) wind turbine system for Low Voltage Ride-Through (LVRT) with a dc chopper. (GSC: Grid-side converter; RSC: Rotor-side converter).

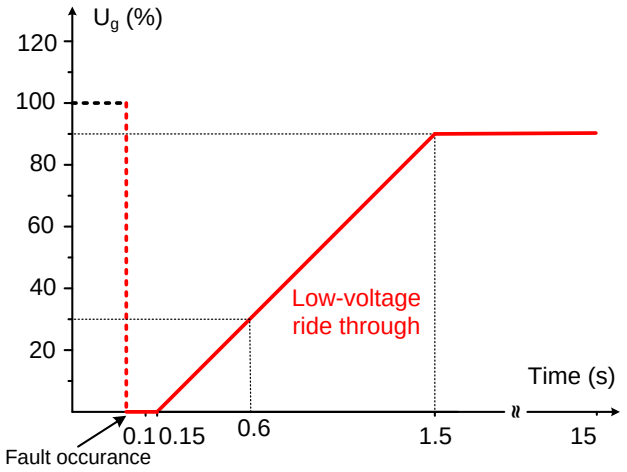

(a)

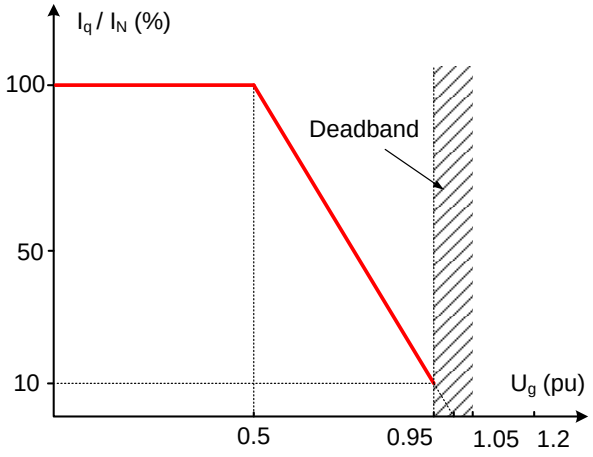

(b)

Fig. 2. Wind turbine requirements under grid disturbance [8]. (a) Voltage ride-through; (b) Reactive current injection during ride-through.

During the symmetrical voltage dip, the newly introduction of the natural flux stands still in respect to the stator winding, which implies that it rotates with the rotor speed ω_r in respect to the rotor winding. In contrast, the normal positive stator flux is rotating with synchronous speed ω_0 in respect to the stator winding, which means that it rotates with the slip speed ω_s in respect to the rotor winding. Meanwhile, the rotor speed is generally 5 times higher than the slip speed at the rated wind speed. As the Electro-Motive Force (EMF), caused by the stator flux viewed from the rotor side, is proportional to the slip speed in normal operation, but to the rotor speed once the symmetrical grid fault happens [12], it can be inferred that the induced rotor voltage becomes much higher, which may cause an over-voltage of the rotor converter, and even induces over-current problem due to the loss of the current control.

According to the modern grid codes [8], the DFIG system is required to overcome above mentioned internal challenge, where the DFIG has to operate for the certain period of the fault without tripping. If the dip level p is defined as,

$$p = \frac{U_{fault}}{U_s} \tag{1}$$

where U_{fault} denotes the grid voltage during the fault period, and U_s denotes the original grid voltage. It is noted that the dip level varies from 0 to 1, and higher dip level indicates severer grid fault.

As shown in Fig. 2(a), it is noted that the severe dip level demands for a shorter survival time. Besides, the DFIG is also expected to provide the reactive power support [8], which can be considered as an external challenge. As shown in Fig. 2(b), it can be seen that the higher dip level needs larger reactive current, in which up to 1.0 pu reactive current is demanded if the voltage dip level is higher than 0.5.

III. DFIG Capability Facing Symmetrical Voltage Dip

This section is dedicated to theoretically analyze and calculate the capability of the DFIG to ride through the symmetrical grid fault.

As discussed in [11]-[13], the demagnetizing control is regarded as the most effective way to overcome the transient period of the natural stator flux decaying due to the fact that the preferred current is solely used to absorb the inductive reactive power introduced by symmetrical grid fault. As shown in Fig. 3, the basic idea of the demagnetizing control is to control the rotor current in the opposite direction in

respect with the natural stator flux. In the d-q axis, the natural flux φ_{sn} (rotating with the synchronous speed ω_0) is extracted from the total stator flux φ_s (dc component and rotating with the synchronous speed ω_0) with the help of a band-pass filter. By the definition of the negative demagnetizing coefficient k, the modulated rotor voltage u_r^* can be obtained by using a traditional PI controller. However, the design of the optimum demagnetizing coefficient is seldom discussed. This paper will evaluate this value seen both from safe operation of the rotor converter and the grid codes requirement. Besides, the minimum junction temperature swing of rotor converter is another important concern.

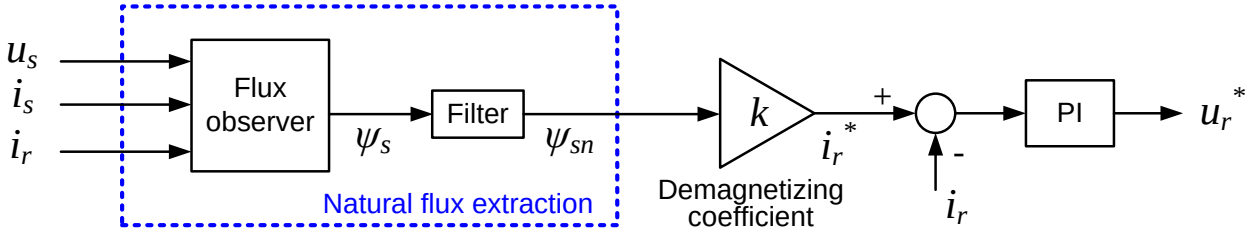

Fig. 3. Control diagram for demagnetizing control strategy.

Table I. GENERATOR SPECIFICATION

Rated power	2 MW
Operational range of rotor speed	1050-1800 rpm
Rated amplitude of stator phase voltage	563 V
Rated frequency	50 Hz
Stator resistance	1.69 mΩ
Rotor resistance	1.52 mΩ
Mutual inductance	2.91 mH
Stator leakage inductance	0.04 mH
Rotor leakage inductance	0.06 mH
Ratio of stator winding and rotor winding	0.369

Table II. ROTOR-SIDE CONVERTER SPECIFICATION

Rated power	400 kW
Rated amplitude of rotor phase current	915 A
Rated amplitude of rotor phase voltage	305 V
Dc-link capacitor	20 mF
Dc-link voltage V_{dc}	1050 V
Switching frequency f_{sw}	2 kHz
Used power module in each arm	1 kA/1.7 kV; two in parallel

A case study is performed in a 2 MW wind turbine system, and the important parameters of the generator and the Rotor-Side Converter (RSC) are shown in Table I and Table II, respectively. In respect to the Safety Operation Area (SOA) of the rotor converter, it is largely dependent on the capacity of the power semiconductor. Due to the power device capacity as well as the rated rotor current and voltage listed in Table II, it can be noted that the RSC can support up to 2.0 pu rotor current. Moreover, if a full modulation index is assumed, 1050 V dc-link voltage is transformed at 2.0 pu rotor voltage. For a 1.7 kV power module, the dc-link voltage should be limited at 1300 V, then 2.5 pu rotor voltage is regarded as the limitation of the voltage stress.

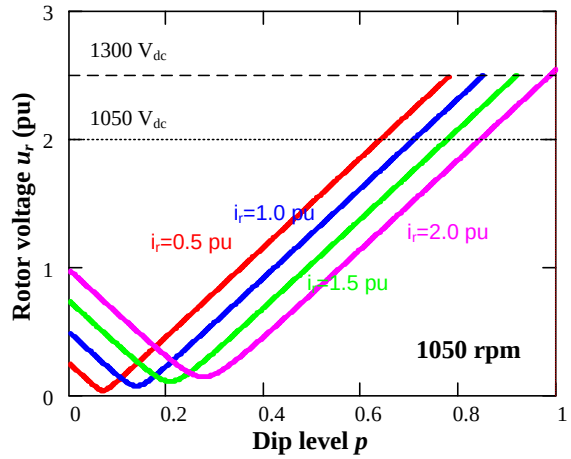

(a)

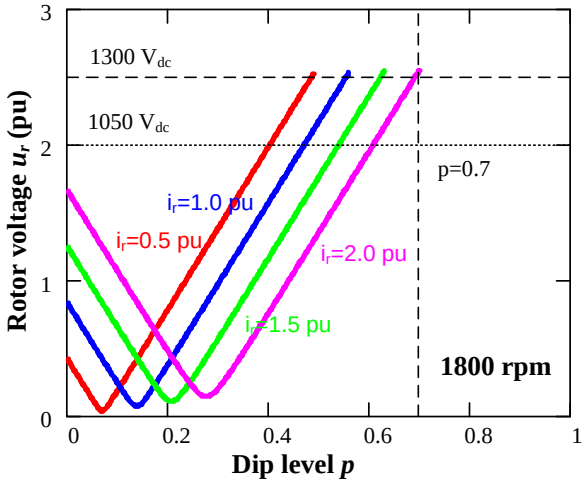

(b)

Fig. 4. Capability of doubly-fed induction generator to ride through various dip levels. (a) 1050 rpm; (b) 1800 rpm.

As discussed in [12], if the demagnetizing current control is applied, the rotor voltage u_r can be expressed in terms of the rotor current i_r,

$$u_r = \omega_r(\sigma L_r i_r - \frac{p \cdot U_s}{\omega_0}) + j(R_r + R_s)i_r \quad (2)$$

where U_s denotes the original stator voltage, R_r and R_s denote the rotor and stator resistance, and σL_r denotes the rotor transient inductance. It is noted that the rotor voltage is not only related to the amount of the demagnetizing current, but also the dip level p as well as the rotor speed ω_r.

If the demagnetizing current is applied from 0.5 pu to 2.0 pu, the characteristics of the rotor voltage and voltage dip level are shown in Fig. 4, in which the minimum speed (1050 rpm) and maximum rotor speed (1800 rpm) are taken into account. It is clear that, at rotor speed of 1050 rpm, the DFIG can fully ride through the symmetrical grid fault, if a 2.0 pu demagnetizing current is provided. However, at a rotor speed of 1800 rpm, although 2.0 pu demagnetizing current is used, the DFIG can only survive within voltage dip level of 0.7. Consequently, the following study will focus on the dip area within 0.7. Besides, it is also noted that the higher demagnetizing current is preferred, the easier for the DFIG to withstand the grid fault.

IV. Control Strategy for Minimum Junction Temperature Swing

In this section, a design procedure of the demagnetizing coefficient will be introduced. It starts with the approach to estimate the thermal behavior from the loading the power semiconductor. Then, the effects of the reactive current response required by the grid codes and residual demagnetizing current at the instant of the reactive current injection are both taken in account. Finally, an optimized demagnetizing coefficient is designed in respect to the minimum junction temperature swing.

A. Approach to estimate thermal behavior

In order to predict the junction temperature of the power semiconductor from the rotor current and rotor voltage, two major transformations will be went through – loss model and thermal model of the power semiconductor [14]. Loss distribution between the IGBT P_T and the freewheeling diode P_D can be obtained with the loss model, and then the junction temperature of IGBT T_{j_T} and the diode T_{j_D} can be estimated based on the thermal model.

Loss dissipation of the power semiconductor mainly consists of the conduction loss and the switching loss, and both of them can be calculated within every fundamental frequency. For the conduction loss, it is the product of the fundamental frequency and the sum of conduction energy by every switching period. The conduction energy is the product of the rotor current I_r, on-state duration time (related to dc-link voltage V_{dc}, rotor voltage U_r and the phase angle between rotor voltage and rotor current), and the voltage drop across the device (V_{ce} for the IGBT and V_f for the diode). For the switching loss, it is the product of the fundamental frequency and the sum of switching energy by every switching period, where the IGBT includes the turn-on E_{on} and turn-off E_{off} switching energy, while the freewheeling diode only has the reserve-recovery energy E_{rr}.

The junction temperature of the power device is decided by the thermal impedance – thermal resistance and thermal time constant (R_T and τ_T for the IGBT, and R_D and τ_D for the diode). Both of them usually consist of the power module itself (from junction to baseplate or case), the thermal interface material as well as the cooling method.

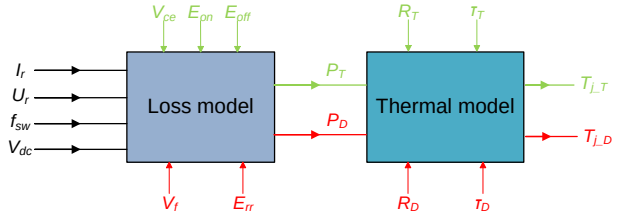

Fig. 5. Approach to estimate the junction temperature of power semiconductor.

As shown in Fig. 5, the thermal behavior of the IGBT and the diode can be calculated with the help of the loss model and thermal model of the power semiconductor. The relevant parameters from the device loading to the junction temperature estimation are listed in Table III. Since the dc-link voltage and the switching frequency are normally kept constant during the operation, it can be inferred that the junction temperature of the power semiconductor is roughly determined by the amplitude of the rotor current.

Table III. Parameters Used in Loss Model and Thermal Model of Power Semiconductors

		IGBT	Diode
Loss model	V_{ce} @ 1 kA, T_j=150 ºC (V)	2.45	/
	V_f @ 1 kA, T_j=150 ºC (V)	/	1.95
	E_{on} @ 1 kA, T_j=150 ºC (mJ)	430	/
	Eo_{ff} @ 1 kA, T_j=150 ºC (mJ)	330	/
	E_{rr} @ 1 kA, T_j=150 ºC (mJ)	/	245
Thermal model	Four order thermal resistance R (ºC/kW)	0.3	0.48
		1.6	3.61
		18	34.6
		3.1	6.47
	Four order thermal time constant τ (s)	0.003	0.0002
		0.0013	0.0009
		0.04	0.03
		0.4	0.2

B. Effect of reactive current injection

According to Fig. 2, the modern grid codes require the wind turbine not only to be connected, but also to provide

certain amount of the reactive current as soon as possible. Different countries demand various response time, and if Spanish grid code is used, a 150 ms response time is specified [8], [9].

For the DFIG configuration, the additional reactive current is normally injected from the stator of the induction generator. It causes an extra current stress seen from the rotor-side [14], [15],

$$i_{r\_Q} = -\frac{(1-p)\cdot U_s}{\omega_0 L_m} - \frac{L_s}{L_m}\cdot i_{s\_Q} \tag{3}$$

where L_s and L_m denote the stator inductance and the mutual inductance, U_s denotes the original stator voltage, i_{s_Q} and i_{r_Q} denote the stator current and rotor current in the q-axis, which are both related to the reactive power.

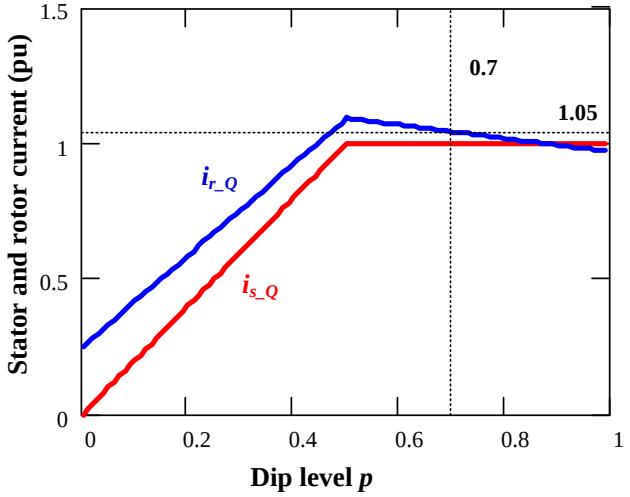

Fig. 6. Requirement of reactive current injection in terms of stator current and rotor current.

Fig. 6 shows the effect of the dip level on the stator current and rotor current. It can be seen that the stator current is kept constant if the dip level is higher than 0.5, while the rotor current reaches the highest value in the case of the dip level of 0.5. As the DFIG can only ride through the dip level up to 0.7, 1.05 pu reactive current needs to be injected from the rotor side.

C. Effect of residual demagnetizing current

If the demagnetizing control is applied, another component of the rotor current during the grid fault is the residual demagnetizing current, and it is closely related to the stator damping constant,

$$\tau = \frac{L_s}{R_s}\cdot\frac{1}{1+\frac{L_m\cdot\omega_0}{p\cdot U_s}\cdot i_r} \tag{4}$$

where τ denotes the time constant of the stator damping. It is noted that the stator damping constant is affected by the amount of the demagnetizing current. Moreover, regardless of the rotor speed, the damping time constant is only related to the dip level and demagnetizing current.

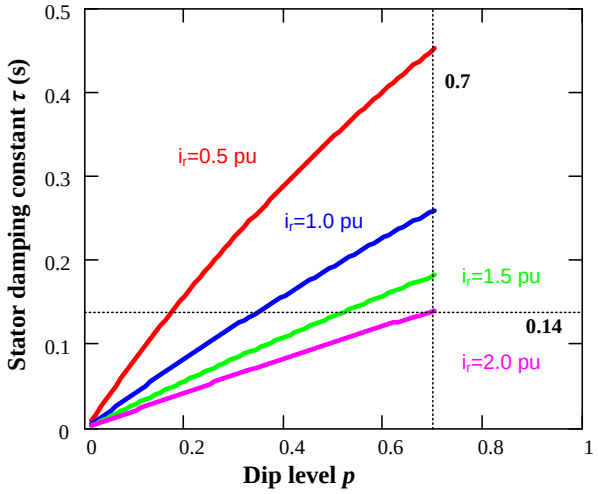

Fig. 7. Demagnetizing current influence on natural flux decaying with various voltage dip levels.

Demagnetizing current influence on natural flux decaying is shown in Fig. 7 with various dip levels. It is obvious that at the same dip level, a higher demagnetizing current causes a faster decaying of the stator natural flux. Besides, higher dip level induces longer transient period at the same demagnetizing current. Specifically, if a 2.0 pu demagnetizing current is selected, the decaying time constant can be reduced from 1750 ms to 140 ms, which significantly shortens the flux transient period.

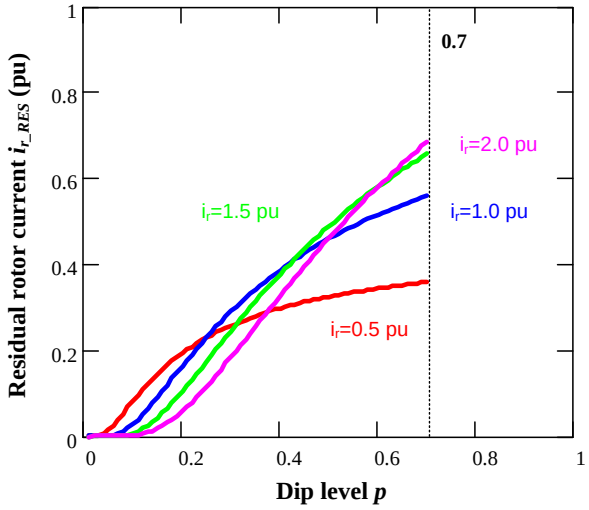

Fig. 8. Residual demagnetizing current at the moment of the reactive current injection.

Simultaneously, the residual demagnetizing current exponentially i_{r_RES} decays during the fault period, and it is expressed as,

$$i_{r\_RES} = i_{r\_DEM} \cdot \exp(-\frac{t_Q}{\tau}) \quad (5)$$

where i_{r_DEM} denotes demagnetizing rotor current at the instant of the fault occurrence, and t_Q denotes the instant when the reactive current is needed.

Consequently, the residual demagnetizing current is shown in Fig. 8 in relation with the voltage dip. It can be seen that although the stator flux can be eliminated sooner with higher amount of demagnetizing current, the residual rotor current is higher at the instant of reactive current injection, which may also cause the power semiconductor more stressed.

D. Optimum demagnetizing coefficient

The suitable demagnetizing current can successfully ride through the grid fault, and it is also able to provide the reactive current on time. Furthermore, the minimum junction temperature swing can be achieved from the power device thermal stress of the point of view.

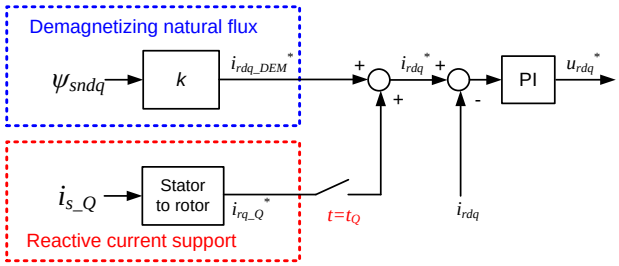

Fig. 9. Control strategy of the rotor-side converter during the grid fault.

The control strategy of the RSC during the grid fault is graphically shown in Fig. 9. Once the fault is detected, the demagnetizing current is provided immediately. At the instant of the reactive current injection t_Q, an additional component of the reactive current is expected other than the exponential decaying of the demagnetizing current. Seen from the similar current loading of the power converter, the optimum demagnetizing coefficient is obtained if the amplitude of the total rotor current at the instant of the reactive current injection equals the amplitude of the maximum demagnetizing current (the instant of the grid fault occurrence).

Summing up the reactive component and demagnetizing component of the rotor current, the relationship between the total rotor current i_{r_TOT} and the demagnetizing current at the instant the reactive power response i_{r_DEM} is shown in Fig. 10, in which the dip levels of 0.7 and 0.2 are used. It can be seen that in order to keep the same amount of the rotor current between the fault occurrence and the instant of the reactive current injection, different demagnetizing coefficients are expected in the case of various voltage dip levels. Specifically, 0.77 pu demagnetizing current is the optimum value at the 0.2 voltage dip, while 1.73 pu demagnetizing current is the best choice for the 0.7 voltage dip.

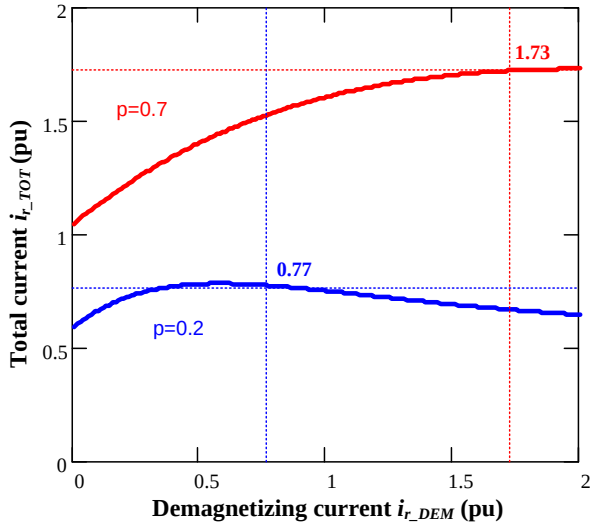

Fig. 10. The relationship between total rotor current and demagnetizing current when the grid fault happens.

V. SIMULATION RESULTS

In order to prevent the power module from a too high dc-link voltage, a dc-brake is used in the simulation and in a real system, whose threshold values for turn-on and turn-off the switch are set at 1300 V and 1100 V by using a hysteresis control [10].

Assuming that a 0.7 balanced grid voltage dip occurs at the instant of 0.5 s, a comparison between the traditional vector control and optimized demagnetizing current control are shown in Fig. 11, in which the DFIG operates with rotor speed at 1800 rpm. For the traditional vector control as shown in Fig. 11(a), once the grid fault is detected, both the active current and reactive current are cut to zero. However, due to the existence of the natural flux, the rotor current (i_{rd} and i_{rq}) cannot track the reference of the rotor current (i_{rd}^* and i_{rq}^*), and the enable time of the dc chopper almost lasts 90 ms. Moreover, in accordance with the grid codes, a 1.0 pu reactive current is injected at the instant of 0.65 s, and the maximum junction temperature of the diode appears during the period without the reactive current injection, which almost reaches 93.0 ºC. As shown in Fig. 11(b), when the grid fault occurs, a 1.73 pu demagnetizing current is selected according to the previous analysis in Fig. 10. During the fault period, the rotor current is almost kept within the desired value, and the enable time of the dc chopper is reduced to 35 ms. Besides, compared with the period of demagnetizing control and reactive current injection, it is noted that the diode is almost equally stressed and its maximum junction temperature is reduced to 90.0 ºC. Furthermore, the damping of the stator flux ψ_s is much faster than the traditional vector control.

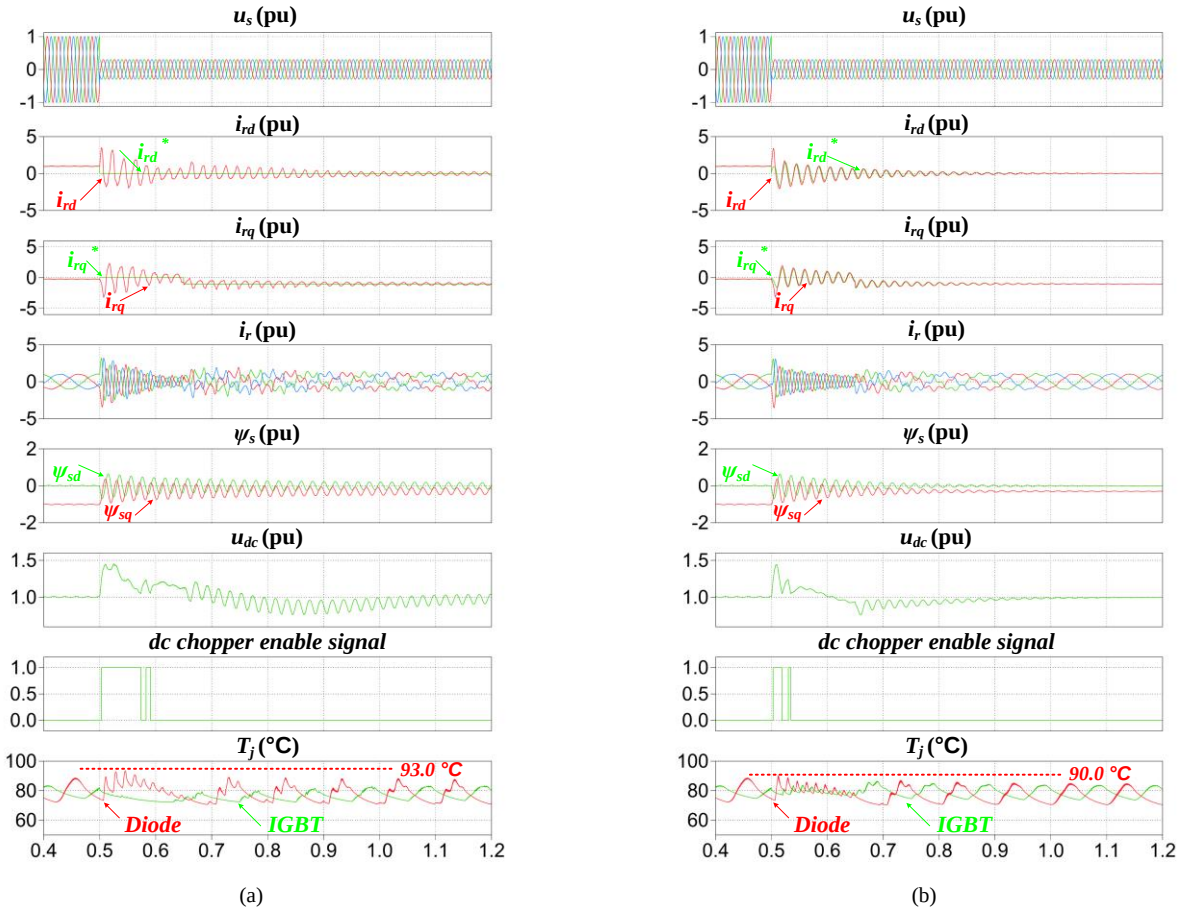

Fig. 11. Simulated results in the case of the DFIG at 1800 rpm to ride through 0.7 dip balanced grid fault with various control schemes. (a) Traditional vector control; (b) Optimized demagnetizing control.

In the case of the rotor speed at 1050 rpm, the simulation result is shown in Fig. 12. Before fault happens, it is noted that the power semiconductor is much lower stressed than 1050 rpm due to the fact that smaller active power is transferred from the RSC. If the traditional vector control is applied as shown in Fig. 12(a), the dc-chopper is triggered for a short period, which indicates it causes dc-link over voltage. Besides, since it is easier for the RSC to ride through grid fault at lower rotor speed as analyzed in Fig. 4, the rotor current is fluctuating within 1.0 pu when grid fault happens. However, the maximum junction temperature occurs during the period of reactive current injection, which eventually reaches 74.0 ºC together with the effects from the residual natural stator flux. If a 1.73 pu demagnetizing current is selected as shown in Fig. 12(b), the maximum junction temperature can be reduced to 70.0 ºC, where the maximum junction temperature between the instant of the fault occurrence and duration of reactive current injection is almost the same.

VI. Conclusion

This paper starts with the existing issues for the doubly-fed induction generator to ride through the symmetrical grid fault. Considering the reactive current injection required by the modern grid codes, by using the conventional demagnetizing current control, a design procedure of the optimum demagnetizing coefficient is proposed in order to realize that maximum rotor current can be kept the same between the fault occurrence and the duration of the reactive current injection. As the thermal behavior of the power semiconductor is mainly decided by its current, this control strategy is able to achieve the minimum junction temperature swing during the low voltage ride-through. It is concluded that, regardless of the rotor speed, the demagnetizing coefficient is only related to the dip level. Simulation results verify the minimum junction temperature swing during the fault period.

References

[1] Danish Energy Agency (website: http://www.ens.dk/en).

[2] H. Wang, M. Liserre, F. Blaabjerg, P. Rimmen, J. Jacobsen, T. Kvisgaard, J. Landkildehus, "Transitioning to physics-of-failure as a reliability driver in power electronics," *IEEE Journal of Emerging and Selected Topics in Power Electronics*, vol. 2, no. 1, pp. 97-114, Mar. 2014.

[3] S. Yang, A. Bryant, P. Mawby, D. Xiang, L. Ran, P. Tavner, "An industrial-based survey of reliability in power electronic converters," *IEEE Trans. on Industrial Applications*, vol. 47, no. 3, pp. 1441-1451, May. 2011.

[4] A. Wintrich, U. Nicolai, W. Tursky, T. Reimann, “Application manual power semiconductors,” Semikron international GmbH, Nuremburg, 2011.

[5] ABB Application Note, Load-cycling capability of HiPaks, 2004.

[6] R. Cardenas, R. Pena, S. Alepuz, G. Asher, "Overview of control systems for the operation of DFIGs in wind energy applications," *IEEE Trans. on Industrial Electronics*, vol. 60, no. 7, pp. 2776-2798, Jul. 2013.

[7] G. Pannell, D. J. Atkinson, B. Zahawi, "Minimum-threshold crowbar for a fault-ride-through grid-code-compliant DFIG wind turbine," *IEEE Trans. on Energy Conversion*, vol. 25, no. 3, pp. 750-759, Sep. 2010.

[8] E.ON-Netz. Requirements for offshore grid connections, Apr. 2008.

[9] M. Tsili, S. Papathanassiou, "A review of grid code technical requirements for wind farms," *IET Renewable Power Generation*, vol. 3, no. 3, pp. 308-332, Sep. 2009.

[10] G. Pannell, B. Zahawi, D. J. Atkinson, P. Missailidis, "Evaluation of the performance of a DC-link brake chopper as a DFIG low-voltage fault-ride-through device," *IEEE Trans. on Energy Conversion*, vol. 28, no. 3, pp. 535-542, Sep. 2013.

[11] D. Xiang, L. Ran, P. J. Tavner, S. Yang, "Control of a doubly fed induction generator in a wind turbine during grid fault ride-through,", *IEEE Trans. on Energy Conversion*, vol. 21, no. 3, pp. 652-662, Sep. 2006.

[12] J. Lopez, E. Gubia, E. Olea, J. Ruiz, L. Marroyo, "Ride through of wind turbines with doubly fed induction generator under symmetrical voltage dips," *IEEE Trans. on Industrial Electronics*, vol. 56, no. 10, pp. 4246-4254, Oct. 2009.

[13] W. Chen, D. Xu, N. Zhu, M. Chen, F. Blaabjerg, "Control of doubly fed induction generator to ride through recurring grid faults," *IEEE Trans. on Power Electronics*, 2015, IEEE early access.

[14] D. Zhou, F. Blaabjerg, M. Lau, M. Tonnes, "Optimized reactive power flow of DFIG power converters for better reliability performance considering grid codes," *IEEE Trans. on Industrial Electronics*, vol. 62, no. 3, pp. 1552-1562, Mar. 2015.

[15] D. Zhou, F. Blaabjerg, T. Franke, M. Tonnes, M. Lau, "Reduced cost of reactive power in doubly fed induction generator wind turbine system with optimized grid filter," *IEEE Trans. on Power Electronics*, vol. 30, no. 10, pp. 5581-5590, Oct. 2015.

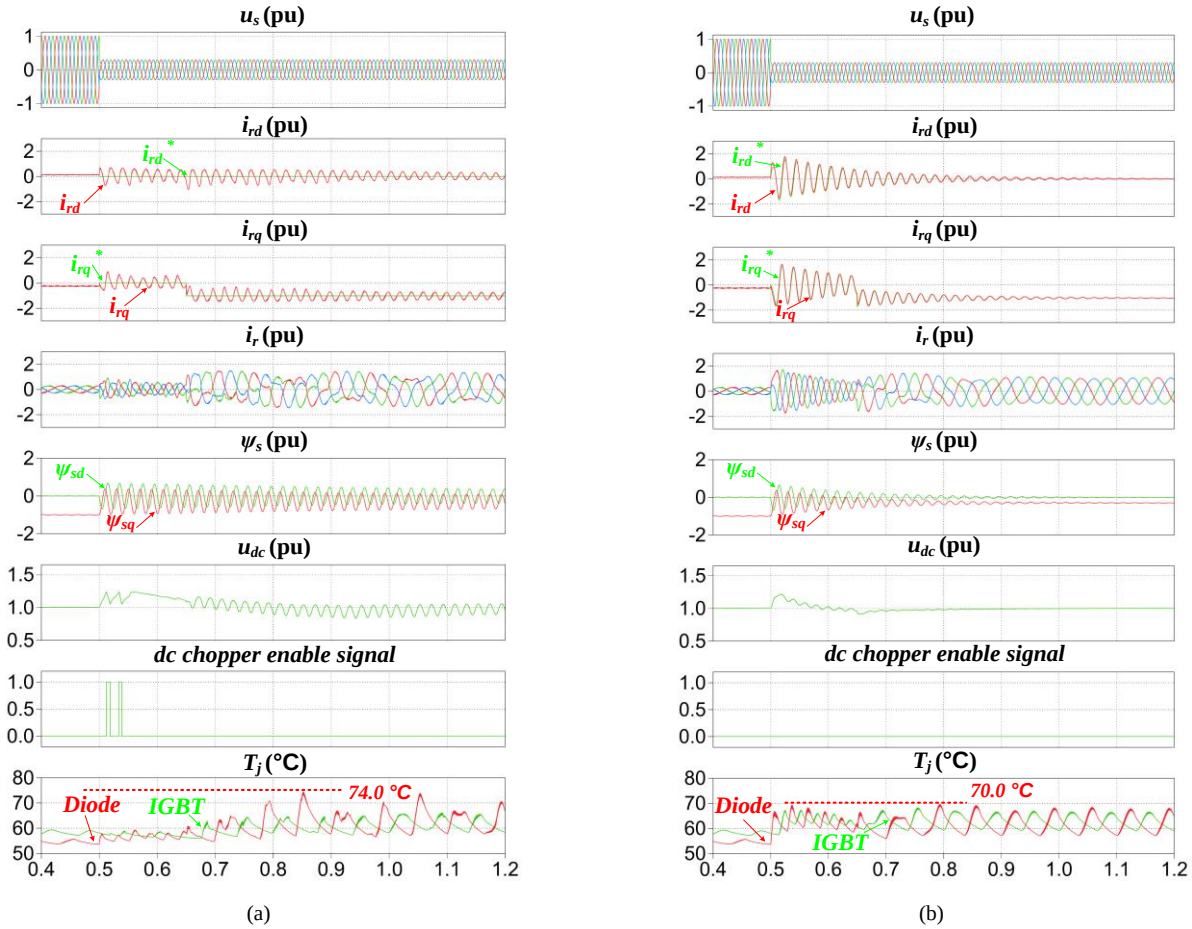

(a) (b)

Fig. 12. Simulated results in the case of the DFIG at 1050 rpm to ride through 0.7 dip balanced grid fault with various control schemes. (a) Traditional vector control; (b) Optimized demagnetizing control.